Molecular Mechanism of Amyloid Inhibition by Inositol

Grace Li[1,2] and Régis Pomès[1,2]
[1]Department of Biochemistry, University of Toronto, Toronto, Ontario
[2]Molecular Structure and Function, The Hospital for Sick Children, Toronto, Ontario

Introduction

One in eight people over the age of 65 has Alzheimer's Disease (AD), a progressive neurodegenerative disease that currently has no cure. The amyloid cascade hypothesis is a long standing hypothesis which states that the extracellular neuronal deposition of Aβ amyloid plaque plays a central role in the pathogensis of AD. Aβ is proteolytically cleaved from the amyloid precursor protein (APP) and is produced as two common alloforms, Aβ40 or Aβ42, which exist in the body normally as monomers. However, in the diseased state, Aβ42 levels are elevated in the body and are found to be the principal component in the deposited Aβ plaques[1,2].

In vitro, both Aβ40 and Aβ42 are intrinsically disordered peptides that self-aggregate to form highly ordered β-sheets organized as a cross-β structure[3]. Moreover, smaller fragments of the full length sequence are also found to form amyloid[4,5]. In particular, the peptide KLVFFAE or Aβ(16-22) is one of the shortest amyloid forming peptides and have been structurally characterized using solid state NMR (ssNMR)[4]. It is believed to be the central hydrophobic core critical for the initiation of aggregation and fibril formation in the full length Aβ peptide[6]. Furthermore, single-point mutations in this region can greatly affect the aggregation propensity of Aβ: known familial AD mutations E22Q (Dutch), E22K (Italian), and E22G (Arctic) significantly accelerate fibril formation[7] where as the mutation F19T abolishes the formation of fibrils *in vitro*[8].

Prior to the appearance of fibrils, amyloidogenic monomers self-aggregate to form a variety of pre-fibrillar intermediate aggregates. While the fibril is an important state implicated in AD, recent research have suggested that soluble oligomers as small as dimers and tetramers play a role in neurotoxicity[9]. In recent years, drug development and research efforts have been directed to the development of therapeutics to prevent the self-aggregation and amyloid formation of Aβ, a promising treatment approach to target the underlying disease. Many different types of *in vitro* amyloid inhibitors have been discovered: peptide[10,11,12,13], immunotherapies[14,15,16], polyphenolic[17,18,19], and small-molecules[17,20,21,22]. These approaches have been reviewed in detail elsewhere in literature[23,24].

Scyllo-inositol is a small molecule amyloid inhibitor developed for treating AD[20,21,23,25,26]. Inositol is a class of polyols with eight stereoisomers commonly found in nature. *Myo*-inositol, the most commonly occurring isomer is found to be highly concentrated in the tissues of the human central nervous system (CNS)[27]. Like *myo*-inositol, *scyllo*-inositol is also present in the brain and can be passively and actively transported across the blood brain barrier[28]. Because of its favorable CNS bioavailability, a main challenge to overcome when developing AD drug candidates, inositol-based therapies represent a unique and promising approach to treating AD. Furthermore, *scyllo*-inositol was demonstrated to prevent and reverse AD-like symptoms in a transgenic mouse model of AD[29]. In 2007, *scyllo*-inositol (ELN0005) was fast-tracked by the United States Food and Drug Administration (FDA) into phase II of clinical trials in North America.

The mechanism of action of *scyllo*-inositol and stereoisomers is not currently understood. *In vitro*, inositol was shown to have stereochemistry-dependent inhibition of Aβ42 fibrils: *myo*-

inositol, *epi*-inositol, and *scyllo*-inositol at 25:1 molar ratio inhibit the amyloid formation of Aβ42, where as *chiro*-inositol is inactive below osmolyte concentrations[25]. It is believed that the likely mechanism of inositol is to inhibit amyloid formation by directly interacting with either monomers or oligomers to 'cap off' fibril growth[25]. The lack of information on the molecular structure of amyloid oligomers have made the experimental determination of the mode of action and binding mode of inositol difficult to achieve. Experimental efforts to characterize the molecular structure of nonfibrillar oligomers are often impeded because of their transient and disordered nature.

The aim of our study is to use explicit solvent unrestrained molecular dynamics simulations (MD) to elucidate the molecular basis of the action of inositol on aggregation pathway of Aβ. Thus far several studies have used MD simulations to gain insight into the binding of peptide-based, and small-molecule inhibitors to fibrillar fragments of Aβ[30,31,32]. However, toxicity is implicated to exist for monomers, oligomers and fibrils, and thus it is important to examine together how a small molecule inhibitor interact with all three of these amyloidogenic states.

In this study, we hypothesize that inositol inhibit fibril formation by directly binding to Aβ peptides and their aggregates. Using Aβ(16-22), we study the binding of inositol by dissecting the complex amyloid aggregation pathway into three main states: the monomer, disordered oligomer and β-oligomer. Systematic comparative MD simulations are carried out with and without *scyllo*- and *chiro*-inositol (the inactive negative control) with each of these species to determine inositol binding equillibria and its effect on aggregation.

Understanding the molecular details of binding sites that are important for inhibition will lead to the prediction and design of better small molecule binders to amyloid and potential therapeutics for amyloid-based diseases. These small molecules will also be useful as imaging agents to detect the presence of prefibrillar aggregates, which can then be applied to assist in the early diagnoses of AD and other neurodegenerative diseases REF.

Results

Binding to the Peptidic Backbone

Alanine dipeptide

Inositol is a polyhydroxyl with six hydroxyl groups capable of making maximally twelve hydrogen bonds with water molecules (Figure 1). We initially hypothesized that a mode of action of inositol is to disrupt hydrogen bonding between aggregating peptides by binding to the backbone. Using alanine dipeptide as a model of the peptidic backbone, we characterized in detail the local backbone binding modes of inositol and the effect of binding on its conformational equilibrium.

We ran a set of unrestrained MD simulations of alanine dipeptide in water to determine the conformational equilibrium of alanine dipeptide in the absence of inositol (Figure 2A). Subsequent set of five independent simulations were carried out for 100 ns with each of *chiro*- and *scyllo*-inositol (inositol:peptide molar ratio of 4:1) (Table 16).

We found that inositol binds weakly (with K_d approx. 1 M) and reversibly to the peptidic backbone by forming one (mono-) or two (bi-dentate) hydrogen bonds. The effect of these binding modes on the backbone conformational equilibrium of the alanine dipeptide were then examined. Overall the global conformational states and their relative populations were not

altered in the presence of inositol. We further computed the relative conformer populations of alanine dipeptide for inositol bound states and found that when inositol is bound bidentate to the backbone, the population of alanine dipeptide β-conformers increased significantly; in contrast, the relative populations of dominant conformers remain unchanged with monodentate binding, suggesting that stereochemistry-independent binding modes of inositol are able to induce local ordering in the peptidic backbone (Figure 2).

Binding to the monomer, disordered and β-oligomer of $(GA)_4$

Following our work with alanine dipeptide, our goal was to probe whether local ordering in the backbone translates into a perturbation of the global conformational equilibrium of an amyloidogenic peptide and whether stereochemistry-independent binding modes were sufficient for inhibition. In the results that follow, we study binding of inositol to the octameric peptide Gly-Ala-Gly-Ala-Gly-Ala-Gly-Ala or $(GA)_4$. $(GA)_4$ is one of the simplest amyloid-like sequences and is found to self-aggregate *in vitro* to form thin, long and flat β-sheets visible by negatively-stained transmission electron microscopy (Simon Sharpe unpublished data). Furthermore, in nature, Gly-Ala repeats are also found in β sheet regions of prion-like peptides[33] and crystalline domains of spider and moth silks[34,35].

Scyllo- and *chiro*-inositol binding equilibrium and binding modes were systematically characterized with a monomer, tetramer and a β-sheet aggregate of $(GA)_4$ (See Table 16 for a summary of the simulation parameters). We measured dissociation constants of 383 +/- 7 mM, 86 +/- 8 mM, and 60 +/- 5 mM for inositol to the monomer, oligomer and protofibrillar aggregates of $(GA)_4$ respectively. We found that binding did not alter the global conformational equilibrium of $(GA)_4$, as measured by the peptide's end-to-end distance distribution. As

expected, binding modes did not differ between scyllo- and chiro- as we had previously found that backbone binding is independent of stereochemistry.

Although the *(GA)$_4$* protofibrillar aggregate presented a much larger surface area for binding than the disordered oligomer, inositol binding is still relatively weak. The *(GA)$_4$* protofibril has a solvent exposed backbone surface where inositol can bind to and locally disrupt backbone-backbone hydrogen bonds. However, inositol molecule binding is constrained by geometry and can make at most two hydrogen bonds at the surface (Figure 3).

From our results so far, we have not found a difference in binding and a difference in activity between chiro- and scyllo-. Thus we conclude that the dominant binding mode of inositol is not only through backbone, and hypothesize that inositol acts through sequence-specific interactions with the Aβ peptide.

Binding to Aβ(16-22)

In the following sections, we use similar simulation approaches to examine inositol binding with the monomer, disordered oligomer and protofibrillar states of the Aβ specific sequence Aβ(16-22).

Binding to the monomer

One possible way a small molecule inhibitor may work is by binding and sequestering unaggregated monomers Aβ. For example, the small molecule polyphenol EGCG was found to inhibit fibril formation in alpha-synuclein by directly binding to its monomeric form. The *in vitro* study by McLaurin et al showed that upon incubation with *scyllo*-, circular dichroism spectroscopy revealed the formation of β structure in the initially random coil monomeric

Aβ42[36], suggesting that binding monomeric Aβ is a possible mode of action for inositol. Although previously we showed that inositol does not affect monomeric *(GA)*$_4$, the possibility of inositol binding the monomer of Aβ(16-22) cannot be eliminated because of the presence of possible stereochemistry-dependent binding modes with the charged and bulkier nonpolar side chains.

Like the full length Aβ, Aβ(16-22) is also a intrinsically disordered peptide in solution and thus, its conformational equilibrium is represented by many different conformational states. A previous study by Soto, P et al have characterized its conformational landscape using the GROMOS force field[30]. Since different MD force fields have different secondary structural biases[37,38], it was important for us to determine the conformational states of Aβ(16-22) in absence of inositol using our chosen force field, OPLS-AA. We used simulated tempering (ST) MD simulations to obtain the conformational equilibrium of Aβ(16-22) in absence of inositol. ST was previously was shown by our lab to be the most efficient simulation method for sampling the conformational landscapes of small peptides[39].

Simulations in the presence of 2:1 and 15:1 inositol:peptide molar ratios were performed. It is important to note that for computational feasibiliy reasons, our systems have lower inositol:peptide molar ratios than the in vitro study by McLaurin et. al with the inositol and peptide final concentrations two magnitudes higher than those used in experiment. However, our highest molar ratio simulations at 15:1 is just under the 25:1 molar ratio where inhibition of the much longer Aβ42 fibrils were observed.

We obtained a similar dissociation constant for both *scyllo*- and *chiro*-inositol at both 2:1 ($K_{d,M(scyllo)}$ = 216 +/- 2 mM , and $K_{d,M(chiro)}$ = 222 +/- 1 mM) and at 15:1 molar ratio ($K_{d,M(scyllo)}$ =

179 +/- 1 mM, and $K_{d,M(chiro)}$ = 168 +/- 2 mM), indicating weak association of inositol with the monomer (See Table 16 for a summary). Increasing the molar ratio of inositol:peptide by more than 7-fold only decreased the K_d by a factor of 1.2, suggesting that although there is binding cooperativity for a monomer, it is unlikely that inositol act as a drug on the monomer. Further, similar to the $(GA)_4$ monomer study, the conformational equilibrium of Aβ(16-22) is preserved in the presence of inositol including the highest molar ratio (Figure 4A and 4B).

Although the overall conformation of the monomer is not affected, it is still important to elucidate the specific binding modes of inositol to each residue as these binding modes can be relevant for binding in higher order structures of Aβ(16-22). For the rest of this section, because of the similarity between the results of the systems at 2:1 and 15:1 molar ratios, we will only refer to data for the 15:1 molar ratio.

Overall inositol binding to the monomer of Aβ(16-22) is dominated by hydrogen bonding interactions: approximately 80% of inositol molecules bind through forming at least one hydrogen bond (Figure 5). Like with alanine dipeptide and $(GA)_4$, inositol make transient hydrogen bonds to the peptidic backbone of Aβ(16-22) (Figure 5A). In addition, inositol also hydrogen bond significantly to the carboxylate side chain of glutamate (Figure 5A). The ability to bind monodentate or bidentate to the carboxylate group of glutamate, results in a much stronger binding preference to glutamate over lysine.

Nonpolar contacts also play an important role in inositol binding: 20% of bound inositol molecules make nonpolar contacts (Figure 5). In particular, we find that *scyllo*-inositol preferentially bind the phenyl group of F18 and F19 over the aliphatic residues, where as chiro-inositol contacts F with indistinguishable frequency from A21(Figure 6). Further characterizing

the binding geometry of inositol to F revealed that the preferential binding of *scyllo*- to F is due to the existence of a planar face-to-face stacking mode specific to the stereochemistry of *scyllo*-. In contrast, *chiro*- is unable to bind F in this mode because of its two adjacent axial hydroxyl groups. This difference in binding is quantified in Figure 7, where a minimum at $r = 0.45$ and theta=10 degrees exist for *scyllo*-, but not *chiro*-inositol.

In summary, although we found stereospecific binding modes, we did not find a difference in binding affinities of scyllo- and chiro- to the monomer. Further, the high dissociation constants obtained for inositol binding to $(GA)_4$ and Aβ(16-22) thus far suggest that it is unlikely that inositol act as a drug on the monomer of Aβ. In the following, we examine the binding of inositol to a small disordered oligomer and a β-sheet oligomer of Aβ(16-22). In recent years, small soluble oligomeric assemblies have been implicated as the key neurotoxic agent in AD[1,40,41], thus underscoring the importance of elucidating how small molecule may bind to these aggregates.

Binding to the Disordered Oligomer

In literature, many MD studies have focused on examining binding to monomers or fibrillar aggregates, the endpoints of aggregation. However, smaller aggregates - dimers, tetramers have been suggested to have neurotoxicity[9]. To probe the effect of inositol on the early aggregation of Aβ(16-22), we ran sets of independent MD simulations with Aβ(16-22) monomers starting with conformations drawn at random from the pool of structures obtained from our ST simulation of the monomer. The peptides were started mono-dispersed in the simulation box with inositol added at molar ratios of 2:4, 4:1, 45:4. Over the course of the

simulation, the peptides aggregate through inter-chain and intra-chain polar and nonpolar contacts to form a soluble disordered oligomer (Figure 8A).

The overall distribution of secondary structure of the small oligomer in each of the systems remained unperturbed in the presence of inositol, including at the highest molar ratio and concentration of inositol. A significant fraction of the residues in the aggregate were in the coil conformation, with a small fraction of β-sheet residues occurring in some of the systems (Figure 8B).

We further characterized the molecular organization of the aggregate by using interpeptide atomic and hydrogen bonding contacts as a measure of the extent of aggregation. A driving force for the formation of amyloid is the hydrophobic effect[42,43]. We characterized the hydrophobic packing of nonpolar groups of Aβ(16-22) in the oligomer by computing the total number of pairwise inter-peptide nonpolar contacts in the aggregate. In all systems, the total number of interpeptide hydrophobic contacts plateaued at approximately 200 pairwise contacts, suggesting that a particular aggregation state was reached (Figure 9). In our control simulation without inositol and in systems with inositol at 15:4, this total number of contacts was reached at about 30 ns, where as the hydrophobic clustering was delayed by approximately 20 ns at the 45:4 (Figure 9).

For simulations at the 15:4 molar ratio, we found that the hydrophobic packing and interpeptide hydrogen bonding of the peptides were not affected by the presence of inositol. In contrast, at molar ratios of 45:4, where inositol is present at osmolyte concentrations ([inositol] ≈ 200 mM), both hydrogen bonding and nonpolar contacts were decreased overall (Figure 10) and can be correlated to the slowing down of the initial peptide self-aggregation (Figure 9).

We also estimated the dissociation constant of inositol with the disordered oligomer. The disordered oligomer at both the 2:4 and 15:4 molar ratios have similar dissociation constants of $K_{d,DO}$ approximately 30 to 40 mM. Although this constant is much smaller than $K_{d,M}$ (the dissociation constant for the monomer), when $K_{d,M}$ is divided by the number of peptides we find that $K_{d,DO} \approx K_{d,M}/4 \approx 170/4 \approx 43\ mM$. Hence, these results suggest that inositol does not bind small oligomeric aggregates cooperatively. Further, binding does not prevent peptides from aggregating or change the morphology of the formed aggregates.

Binding to a β-oligomer

Our results so far indicate that the monomer and small disordered oligomers are not likely interaction partners of inositol. Here we examine the binding of inositol to a ordered protofibrillar-like aggregate that we will refer to as the β-oligomer from here on. In our simulations, the oligomer maintained a stable β-sheet core both in the presence and absence of inositol. Furthermore, beginning at about 10ns, the initially rectangularly stacked sheets evolved into a twisted β-sheet structure with interstand twisting along the long axis of the fibril and a slight intersheet twist. The resulting structure has an average twist angle of approximately 25 degrees for the 'top' sheet and 15 degrees for the bottom sheet (Figure 11C). Similar twisting have also been observed for oligomers for Aβ(16-22) in other simulation studies and oligomers of other model peptides[30] and are presumed to contribute to the overall stability of the aggregate.

In our simulations at a molar ratio of 64:4, at the sub-osmolar concentration ([inositol] = 70 mM), K_d of 3 *mM* (+/- 2 mM) was obtained for *scyllo*- and *chiro*-inositol. Here, unlike in our previous studies with (GA)4 and other aggregation states, we found that inositol is able to bind β-oligomers at the required inositol concentration for activity *in vivo* (mice) and *in vitro* (1

mM - 5 mM) [25,29]. Thus, our results here suggest that the β-oligomer is a possible structural analogue of an *in vitro* binding partner of inositol.

We claim that the β-oligomer of Aβ(16-22) have the features that are specific for inositol binding. The exposure of many charged groups at the surface of the oligomer, especially that of glutamate promotes inositol binding. In Figure 12 the per residue inositol contact map shows the residues in the region where inositol binds: inositol has the highest contacts with charged residues glutamate, lysine, and nonpolar residues phenylanine. This is reminiscent of protein-sugar binding sites where aromatic residues such as tryptophan, phenylalanine and glutamate are the most common residues to coordinate sugar binding[44,45,46]. However, although we found disruptive binding modes where inositol is able to intercalate between sheets and between strands, we did not find any disaggregation of the preformed β-oligomer in our simulations.

The high degree of twisting present in the β-oligomer contributes to the overall increased binding by creating tight grooves that allow for stable interactions with inositol. Interestingly, the degree of twist that we observe is much higher than that of amyloid fibrils from experiment, which were found to only exhibit mild twisting[47,48]. In contrast, a commonly used amyloid dye, Thioflavin T (ThT) was shown to favor binding to flat and rigid surfaces found on amyloid fibrils instead of highly twisted sheets. Because inositol can bind to different aggregates from ThT, suggests that inositol may serve as a potential detector for oligomeric states that currently cannot be visualized using amyloid dyes.

The spatial probability density of bound inositol (at [inositol] = 200 mM) shows that both *scyllo*- and *chiro*-inositol bind and coat exposed amphipathic surfaces of the highly twisted β-sheets (Figure 13). These amphipathic regions are found on the faces of the oligomer sheets, where as larger hydrophobic areas are solvent exposed at the strand edges. Although there is no

difference in the global spatial distribution of *scyllo*- and *chiro*-inositol around the β-oligomer, we find that a significantly higher number of *scyllo*- bind by forming nonpolar contacts than *chiro*-, suggesting that *scyllo*- is more competent than *chiro*- in solubilizing nonpolar groups (Figure 13E).

Finally, inositol exhibits binding cooperativity with the β-oligomer (Figure 14). Whereas $K_{d,BO} \approx 3\ mM$ at the 64:16 molar ratio of inositol:peptide, a $K_{d,BO} \approx 18$ mM at the lower molar ratio of 4:16. Examples of such binding modes are shown in Figure 14A and 14B. A overall comparisons of all of the dissociation constants computed in this study is shown in Figure 15.

Discussion and Conclusions

Increasing number of literature have been published on *in vitro* amyloid inhibition effects of many different small molecules, yet there is a lack of a molecular understanding of why and how these molecules work. In our study, we have demonstrated how inositol stereoisomers, a class of sugar-like polyols, are able to binding to amyloidogenic peptides and aggregates. We have dissected the various possible interactions and binding modes of inositol with three representative states along the aggregation pathway: the monomer, disordered oligomer and a protofibrillar β-sheet like oligomer. Although our study examined binding to KLVFFAE, a short stretch of Aβ40 or Aβ42, our minimalist models were able to capture the neccessary interactions to achieve the experimentally observed minimal concentration required for activity and identify possible binding partners and binding sites for inositol.

Specifically, we found that both *scyllo*- and *chiro*-inositol bind to soluble β-sheet oligomers of KLVFFAE and do not act on either monomers or very small disordered oligomers. Inositol binding involves both hydrogen bonding and nonpolar interactions that are specific to

the particular surface chemical environment imparted by the sequence that the aggregate is composed of. Our results indicate that a likely *in vitro* inositol bound amyloid state is a β-sheet like prefibrillar oligomer similar in ultrastructure and surface properties to the β-oligomer of KLVFFAE that we have simulated in our study. A recent study on the effect of *scyllo*-inositol treatment on the hippocampal long term potentiation in rats suggested that *scyllo*-inositol may bind trimers of Aβ[49]. Our results do not preclude the possibility of inositol binding oligomers of the much longer Aβ with less number of peptides.

Many previous studies have highlighted the common presence of planar aromatic rings and multiple hydrogen bonding groups in small molecule inhibitors and suggested that they may be key features for their activity[31,50]. Our study showed that inositol molecules, although non-aromatic also contain potent features for amyloid binding. In particular, CH-π interactions between the cyclohexane ring of inositol and aromatic side chains on the amyloid can drive inositol binding to amyloid, while hydroxyl groups coordinate multiple hydrogen bonds with nearby charged / polar chemical groups.

Furthermore, results from *in vitro* studies have suggested a strong correlation between the variation in the arrangement of hydroxyl groups around the cyclohexane ring and the activity of the inositol stereoisomer. Our results suggest a possible molecular basis of this structure activity relationship: the difference in stereochemistry leads to a difference in binding modes with planar aromatic side chains and / or exposed hydrophobic surfaces. However, despite its lack of nonpolar faces, we found that *chiro*- can still bind with similar affinity as *scyllo*- to KLVFFAE.

Our study suggests that Aβ amyloid aggregates may contain binding sites that are characteristically sugar-like[44]. This finding raises the interesting possibility of the presence of

sugar-like binding sites in amyloid fibrils in general, which can be exploited to design novel amyloid inhibitors and imaging agents. Thus, inositol and inositol-derived small molecules represent a promising class of new drugs with good bioavailability and low toxicity for the treatment of amyloid-based disorders such as AD[26].

Amyloid is hypothesized to growth by either strand addition along the long axis of the fiber or by lateral association with other peptides and oligomers REF. KLVFFAE is known to be incorporated in the β-sheet core of the full length Aβ42 fibril and have been suggested to be at the interface between two separate protofilaments[3]. Our finding that inositol is able to bind cooperatively at the surface of small β-sheet like oligomers suggest that inositol may disrupt lateral growth of prefibrillar fragments. Thus, our results suggest an Aβ specific mechanism by which fibril formation can be abolished by binding early prefibrillar oligomers.

A chemically similar compound to inositol that also inhibit fibril formation is trehalose[51], a disaccharide that is a well-known osmolyte and cryoprotectant. However, trehalose does not inhibit the aggregation and formation of Aβ42 oligomers, the major component in AD and was suggested to inhibit amyloid aggregation of Aβ40 through osmolyte effects.

An unexpected aspect of our study is the lack of a difference in the binding affinity between *scyllo*- and *chiro*- despite their differences in stereochemistry and activity found *in vitro*. Based on evidence from *in vitro* studies and our own simulation results, there are several possibilities for this lack of a difference. First, it is possible that *scyllo*- and *chiro*- have a similar mode of action on the aggregation of Aβ(16-22): they either both do not act to inhibit the amyloid formation of Aβ(16-22) or they both suppress Aβ(16-22) fibril formation. In either case, the results from our simulations are still relevant and predictive of inositol binding modes

with aggregates of full length Aβ. The milimolar dissociation constant measured in our simulation suggests that binding of inositol with the β-oligomer of Aβ(16-22) captures the approximate binding affinity at which inositol is physiologically active. Although our study does not directly speak to whether inositol is able to inhibit the amyloid formation by KLVFFAE, biophysical experiments based on the hypotheses that we put forth in this study are currently underway.

Another possibility to explain the similarity in binding affinity between scyllo- and chiro-inositol is that the empirical force fields of MD simulations may not capture all of the forces involved in inositol-protein binding. CH-π interactions are weak dispersion forces important for carbohydrate recognition by aromatic residues in proteins[52]. However, these are only modeled as Van der Waals interactions in empirical MD forcefields and the differences in the ability of a particular inositol stereoisomer to form CH-π bonds is not dependent on the distribution and orientation of the hydroxyl groups around the cyclohexane ring. It may be useful to perform *ab initio* calculations to reparameterize inositol molecules to better account for these interactions. Nevertheless, in our study we have shown that MD simulations with empircal force fields are capable of identifying stereospecific binding modes with Aβ, interaction partners and binding constants for inositols, a novel class of amyloid inhibitors.

Materials and Methods

Parameterization of inositol molecules

The partial charges, bond, dihedral and angle parameters were taken from the OPLS-AA parameters for carbohydrates[53].

Molecular dynamics simulations

MD simulations were performed with OPLS-AA forcefield in the Gromacs MD simulation package[54,55](version 3.3.1 and versio 4.0.x), where the TIP3P water model was used. Berendsen algorithm was using to control the temperature at T=300K and pressure at 1 atm.

Alanine dipeptide

Simulations at a peptide to inositol molar ratio of 1:4, with a inositol concentration of 250mM were done with alanine dipeptide. Note that the same methods for simulations of (GA)4 are used with Aβ (16-22).

Aβ(16-22)

monomer

We used the simulated tempering algorithm with molecular dynamics to obtain the conformational equilibrium of Aβ(16-22) and used the ensemble of structures at 300K to initiate our simulations with inositol. Inositol molecules were added at molar ratios of inositol:peptide at 2:1 to a set of 1200 structures taken from the structural ensemble obtained from the ST simulation at 296 K. Short MD simulations of 5 ns were then performed for each peptide box at T=300 K. Control simulations of each peptide structure were also done in the absence of inositol at T=300 K to compare to the ensemble generated at 300 K with inositol. Simulations at 15:1 were then done on a 500 structure subset of the 1200 structures.

disordered oligomer

The disordered oligomer systems are initially started with four unaggregated Aβ(16-22) monomer structures (drawn from our ST simulation pool of structures). Inositol molecules are added at ratios of 2:4, 15:4, and 45:4.

β-oligomer

We have modeled the β-oligomer as a rectangular, dual-stacked antiparallel β-sheet structure based on solid-state NMR evidence[4]. However, in the NMR study, the β-sheet stacking mode was not identified and thus, we assumed a β-sheet stacking mode where the charged side chains of lysine and glutamate are on the same side of a sheet and are located on the solvent exposed faces of the aggregate. Inositol molecules were added into the system at a inositol:peptide molar ratio of 64:16 at both a concentration of 60 mM and at a saturated concentration of 200 mM.

A set of ten independent simulations were run for both *scyllo*- and *chiro*-inositol and binding to the β-oligomer were monitored over 100 nanoseconds of simulation time for each trajectory. For comparisons, the same set of simulations were repeated at a much lower inositol:peptide molar ratio of 4:16 with a similar concentration, where initial snapshots were extracted from a single 100 ns simulation of the β-oligomer in water. 6 independent systems were ran for 100 ns, and initiated with 4 molecules of chiro- or scyllo-inositol at a concentration of 40 mM.

Analysis

Hydrogen bonding
A hydrogen bond is counted to exist between a pair of donor and acceptor based on the DSSP hydrogen bonding criteria[56].

Nonpolar cutoff
A cutoff of 4.5 A was used for interpeptide nonpolar atomic contacts.

Contact analysis
Nonpolar contacts for each residue is computed as the total number of side chain atom to $COM_{inositol}$ normalized by the total number of chains, atoms in the side chain and number of frames in the trajectory. Fraction of time is computed as the total count of frames with at least 1 contact between inositol and protein normalized by the total number of frames of in the trajectory. At least one nonpolar contact, or hydrogen bond needs to be present between inositol and peptide for the inositol to be considered bound to the peptide.

Binding probability
The probability of forming X=x number of contacts with a protein species S, $P(X = x)$, is defined by the number of S with x hydrogen bonds with inositol normalized by the total number of frames.

Dissociation constants (K_d)
Given the reaction Protein-Inositol <-> Protein + Inositol
The dissociation constant is K_d = [protein][inositol]/[protein-inositol] = (Fraction unbound/Fraction bound)(concentration of free inositol)
K_d is computed directly from the binding probability histograms and is referred to the binding constant of inositol to protein.

End-to-end distribution
The end-to-end distance of a peptide is defined by the distance between the first and the last alpha-carbon in the peptide. The final distribution is computed by discretizing this distance and binning with a bin size of 0.02 A.

Potential of mean force
The PMF for binding of scyllo-inositol and chiro-inositol to sidechain of phenylalanine was computed based on a 2D reaction coordinate, r, the distance between the center of geometry of inositol and phenylalanine sidechain and theta, the angle between the planes of inositol cyclohexane ring and the benzene ring of phenylalanine. A cutoff of 4.5 A is used between center of geometry of its side chain and the center of geometry of inositol molecule to the phenylalanine side chain. The 2D discretized probability distribution, p(r,theta) is then converted to a free energy by W=-RTln p(r,theta).

Error estimates
Errors are calculated by taking the standard deviation of the quantity of interest of each of the independent simulations. Errors are propagated using the appropriate propagation of uncertainty formula.

Bibliography

1. Haass, C. & Selkoe, D. J. (2007). Soluble protein oligomers in neurodegeneration: lessons from the Alzheimer's amyloid beta-peptide. *Nat Rev Mol Cell Biol* **8**, 101-12.
2. Westaway, D., Xia, W., Carlson, G., Diehl, T. & Levesque …, G. (1997). Mutant presenilins of Alzheimer's disease increase production of 42-residue amyloid β-protein in both transfected cells and transgenic mice. *Nat Med*.
3. Petkova, A. T., Ishii, Y., Balbach, J. J., Antzutkin, O. N., Leapman, R. D., Delaglio, F. & Tycko, R. (2002). A structural model for Alzheimer's beta -amyloid fibrils based on experimental constraints from solid state NMR. *Proc Natl Acad Sci USA* **99**, 16742-7.
4. Balbach, J. J., Ishii, Y., Antzutkin, O. N., Leapman, R. D., Rizzo, N. W., Dyda, F., Reed, J. & Tycko, R. (2000). Amyloid fibril formation by A beta 16-22, a seven-residue fragment of the Alzheimer's beta-amyloid peptide, and structural characterization by solid state NMR. *Biochemistry* **39**, 13748-59.
5. Sawaya, M. R., Sambashivan, S., Nelson, R., Ivanova, M. I., Sievers, S. A., Apostol, M. I., Thompson, M. J., Balbirnie, M., Wiltzius, J. J. W., McFarlane, H. T., Madsen, A. Ø., Riekel, C. & Eisenberg, D. (2007). Atomic structures of amyloid cross-beta spines reveal varied steric zippers. *Nature* **447**, 453-7.
6. Wood, S. J., Wetzel, R., Martin, J. D. & Hurle, M. R. (1995). Prolines and amyloidogenicity in fragments of the Alzheimer's peptide beta/A4. *Biochemistry* **34**, 724-30.
7. Murakami, K., Irie, K., Morimoto, A., Ohigashi, H., Shindo, M., Nagao, M., Shimizu, T. & Shirasawa, T. (2003). Neurotoxicity and physicochemical properties of Abeta mutant peptides from cerebral amyloid angiopathy: implication for the pathogenesis of cerebral amyloid angiopathy and Alzheimer's disease. *J Biol Chem* **278**, 46179-87.
8. Esler, W., Stimson, E., Ghilardi, J. & Lu, Y. (1996). Point Substitution in the Central Hydrophobic Cluster of a Human [beta]-Amyloid Congener Disrupts Peptide Folding and Abolishes Plaque Competence†. *Biochemistry*.
9. Bernstein, S., Dupuis, N., Lazo, N. & Wyttenbach, T. (2009). Amyloid-β protein oligomerization and the importance of tetramers and dodecamers in the aetiology of Alzheimer's disease. *Nature Chemistry*.
10. Esteras-Chopo, A., Morra, G., Moroni, E., Serrano, L., Lopez de la Paz, M. & Colombo, G. (2008). A molecular dynamics study of the interaction of D-peptide amyloid inhibitors with their target sequence reveals a potential inhibitory pharmacophore conformation. *Journal of Molecular Biology* **383**, 266-80.
11. Sciarretta, K. L., Gordon, D. J. & Meredith, S. C. (2006). Peptide-based inhibitors of amyloid assembly. *Meth Enzymol* **413**, 273-312.
12. Chalifour, R. J., McLaughlin, R. W., Lavoie, L., Morissette, C., Tremblay, N., Boulé, M., Sarazin, P., Stéa, D., Lacombe, D., Tremblay, P. & Gervais, F. (2003). Stereoselective interactions of peptide inhibitors with the beta-amyloid peptide. *J Biol Chem* **278**, 34874-81.
13. Scrocchi, L. A., Chen, Y., Waschuk, S., Wang, F., Cheung, S., Darabie, A. A., McLaurin, J. & Fraser, P. E. (2002). Design of peptide-based inhibitors of human islet amyloid polypeptide fibrillogenesis. *Journal of Molecular Biology* **318**, 697-706.

14. Solomon, B. & Frenkel, D. (2010). Immunotherapy for Alzheimer's disease. *Neuropharmacology*.
15. von Bernhardi, R. (2010). Immunotherapy in Alzheimer's disease: where do we stand? Where should we go? *J Alzheimers Dis* **19**, 405-21.
16. Janus, C., Pearson, J., McLaurin, J., Mathews, P. M., Jiang, Y., Schmidt, S. D., Chishti, M. A., Horne, P., Heslin, D., French, J., Mount, H. T., Nixon, R. A., Mercken, M., Bergeron, C., Fraser, P. E., St George-Hyslop, P. & Westaway, D. (2000). A beta peptide immunization reduces behavioural impairment and plaques in a model of Alzheimer's disease. *Nature* **408**, 979-82.
17. Masuda, M., Hasegawa, M., Nonaka, T., Oikawa, T., Yonetani, M., Yamaguchi, Y., Kato, K., Hisanaga, S.-i. & Goedert, M. (2030). Inhibition of α-synuclein fibril assembly by small molecules: Analysis using epitope-specific antibodies. *FEBS Letters* **583**, 787-791.
18. Berhanu, W. M. & Masunov, A. E. (2010). Natural polyphenols as inhibitors of amyloid aggregation. Molecular dynamics study of GNNQQNY heptapeptide decamer. *Biophysical Chemistry* **149**, 12-21.
19. Ehrnhoefer, D. E., Bieschke, J., Boeddrich, A., Herbst, M., Masino, L., Lurz, R., Engemann, S., Pastore, A. & Wanker, E. E. (2008). EGCG redirects amyloidogenic polypeptides into unstructured, off-pathway oligomers. *Nat Struct Mol Biol* **15**, 558-66.
20. Hawkes, C. A., Ng, V. & McLaurin, J. (2009). Small molecule inhibitors of Aβ-aggregation and neurotoxicity. *Drug Dev. Res.* **70**, 111-124.
21. Nitz, M., Fenili, D., Darabie, A. A., Wu, L., Cousins, J. E. & McLaurin, J. (2008). Modulation of amyloid-beta aggregation and toxicity by inososе stereoisomers. *FEBS J* **275**, 1663-74.
22. Necula, M., Kayed, R., Milton, S. & Glabe, C. G. (2007). Small molecule inhibitors of aggregation indicate that amyloid beta oligomerization and fibrillization pathways are independent and distinct. *J Biol Chem* **282**, 10311-24.
23. Dasilva, K. A., Shaw, J. E. & McLaurin, J. (2009). Amyloid-β fibrillogenesis: Structural insight and therapeutic intervention. *Exp Neurol*, 1-11.
24. Citron, M. (2010). Alzheimer's disease: strategies for disease modification. *Nat Rev Drug Discov* **9**, 387-98.
25. McLaurin, J., Golomb, R., Jurewicz, A., Antel, J. P. & Fraser, P. E. (2000). Inositol stereoisomers stabilize an oligomeric aggregate of Alzheimer amyloid beta peptide and inhibit abeta -induced toxicity. *J Biol Chem* **275**, 18495-502.
26. Sun, Y., Zhang, G., Hawkes, C. A., Shaw, J. E., McLaurin, J. & Nitz, M. (2008). Synthesis of scyllo-inositol derivatives and their effects on amyloid beta peptide aggregation. *Bioorganic & Medicinal Chemistry* **16**, 7177-84.
27. Fisher, S. K., Novak, J. E. & Agranoff, B. W. (2002). Inositol and higher inositol phosphates in neural tissues: homeostasis, metabolism and functional significance. *J Neurochem* **82**, 736-54.
28. Fenili, D., Brown, M., Rappaport, R. & McLaurin, J. (2007). Properties of scyllo-inositol as a therapeutic treatment of AD-like pathology. *J Mol Med* **85**, 603-11.
29. McLaurin, J., Kierstead, M. E., Brown, M. E., Hawkes, C. A., Lambermon, M. H. L., Phinney, A. L., Darabie, A. A., Cousins, J. E., French, J. E., Lan, M. F., Chen, F., Wong, S. S. N., Mount, H. T. J., Fraser, P. E., Westaway, D. & St George-Hyslop, P. (2006).

Cyclohexanehexol inhibitors of Abeta aggregation prevent and reverse Alzheimer phenotype in a mouse model. *Nat Med* **12**, 801-8.

30. Soto, P., Griffin, M. A. & Shea, J.-E. (2007). New insights into the mechanism of Alzheimer amyloid-beta fibrillogenesis inhibition by N-methylated peptides. *Biophysical Journal* **93**, 3015-25.
31. Lemkul, J. A. & Bevan, D. R. (2010). Destabilizing Alzheimer's Aβ42Protofibrils with Morin: Mechanistic Insights from Molecular Dynamics Simulations. *Biochemistry* **49**, 3935-3946.
32. Raman, E. P., Takeda, T. & Klimov, D. K. (2009). Molecular Dynamics Simulations of Ibuprofen Binding to Aβ Peptides. *Biophysical Journal* **97**, 2070-2079.
33. Walsh, P., Simonetti, K. & Sharpe, S. (2009). Core structure of amyloid fibrils formed by residues 106-126 of the human prion protein. *Structure* **17**, 417-26.
34. Vandermeulen, G. W. M., Kim, K. T., Wang, Z. & Manners, I. (2006). Metallopolymer-peptide conjugates: synthesis and self-assembly of polyferrocenylsilane graft and block copolymers containing a beta-sheet forming Gly-Ala-Gly-Ala tetrapeptide segment. *Biomacromolecules* **7**, 1005-10.
35. Asakura, T., Yamane, T., Nakazawa, Y., Kameda, T. & Ando, K. (2001). Structure of Bombyx mori silk fibroin before spinning in solid state studied with wide angle x-ray scattering and (13)C cross-polarization/magic angle spinning NMR. *Biopolymers* **58**, 521-5.
36. McLaurin, J., Franklin, T., Chakrabartty, A. & Fraser, P. E. (1998). Phosphatidylinositol and inositol involvement in Alzheimer amyloid-beta fibril growth and arrest. *Journal of Molecular Biology* **278**, 183-94.
37. Cao, Z. & Wang, J. (2010). A comparative study of two different force fields on structural and thermodynamics character of H1 peptide via molecular dynamics simulations. *Journal of biomolecular structure & dynamics*.
38. Gnanakaran, S., Nussinov, R. & García, A. E. (2006). Atomic-level description of amyloid beta-dimer formation. *J. Am. Chem. Soc.* **128**, 2158-9.
39. Rauscher, S. N., Chris & Pomes, R. (2009). Simulated Tempering Distributed Replica Sampling, Virtual Replica Exchange, and Other Generalized-Ensemble Methods for Conformational Sampling. *JCTC*, 1-23.
40. Walsh, D. M., Klyubin, I., Fadeeva, J. V., Cullen, W. K., Anwyl, R., Wolfe, M. S., Rowan, M. J. & Selkoe, D. J. (2002). Naturally secreted oligomers of amyloid beta protein potently inhibit hippocampal long-term potentiation in vivo. *Nature* **416**, 535-9.
41. Selkoe, D. J. (1999). Translating cell biology into therapeutic advances in Alzheimer's disease. *Nature* **399**, A23-31.
42. Auer, S., Meersman, F. & Dobson, C. (2008). A generic mechanism of emergence of amyloid protofilaments from disordered oligomeric aggregates. *PLoS Computational ...*.
43. Chiti, F. & Dobson, C. (2006). Protein misfolding, functional amyloid, and human disease. *Annual Reviews*.
44. Taroni, C., Jones, S. & Thornton(2), J. M. (2000). Analysis and prediction of carbohydrate binding sites. *Protein Eng* **13**, 89-98.
45. Kulharia, M., Bridgett, S. J., Goody, R. S. & Jackson, R. M. (2009). InCa-SiteFinder: a method for structure-based prediction of inositol and carbohydrate binding sites on proteins. *J Mol Graph Model* **28**, 297-303.

46. Weis, W. & Drickamer, K. (1996). Structural basis of lectin-carbohydrate recognition. *Annu Rev Biochem*.
47. Lührs, T., Ritter, C., Adrian, M. & Riek- …, D. (2005). 3D structure of Alzheimer's amyloid-β (1–42) fibrils. *Proceedings of the …*.
48. Robinson, C., Dobson, C. & Saibil, H. (2002). The protofilament structure of insulin amyloid fibrils. *Proceedings of the …*.
49. Townsend, M., Cleary, J. P., Mehta, T., Hofmeister, J., Lesne, S., O'hare, E., Walsh, D. M. & Selkoe, D. J. (2006). Orally available compound prevents deficits in memory caused by the Alzheimer amyloid-β oligomers. *Ann Neurol.* **60**, 668-676.
50. Porat, Y., Abramowitz, A. & Gazit, E. (2006). Inhibition of amyloid fibril formation by polyphenols: structural similarity and aromatic interactions as a common inhibition mechanism. *Chemical Biology & Drug Design* **67**, 27-37.
51. Liu, R., Barkhordarian, H., Emadi, S., Park, C. B. & Sierks, M. R. (2005). Trehalose differentially inhibits aggregation and neurotoxicity of beta-amyloid 40 and 42. *Neurobiol Dis* **20**, 74-81.
52. Ramirez-Gualito, K. (2009). Enthalpic Nature of the CH/π Interaction Involved in the Recognition of Carbohydrates by Aromatic Compounds, Confirmed by a Novel Interplay of NMR, Calorimetry, and Theoretical Calculations. 1-10.
53. Kony, D., Damm, W., Stoll, S. & Van …, W. (2002). An improved OPLS-AA force field for carbohydrates. *Journal of …*.
54. Hess, B., Kutzner, C. & van der Spoel, D. (2008). Gromacs 4: Algorithms for highly efficient, load-balanced, and scalable molecular simulation. *J. Chem. Theory …*.
55. van der Spoel, D., Lindahl, E. & Hess, B. (2005). GROMACS: fast, flexible, and free. *Journal of …*.
56. Kabsch, W. & Sander, C. (1983). Dictionary of protein secondary structure: pattern recognition of hydrogen-bonded and geometrical features. *Biopolymers*.

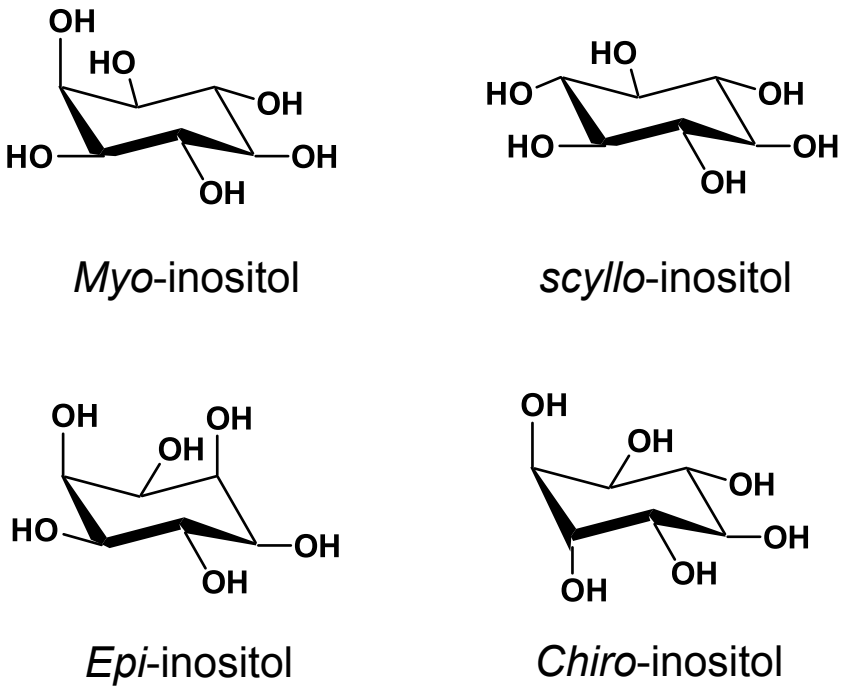

Figure 1: The four most commonly occurring stereoisomers of inositol in nature

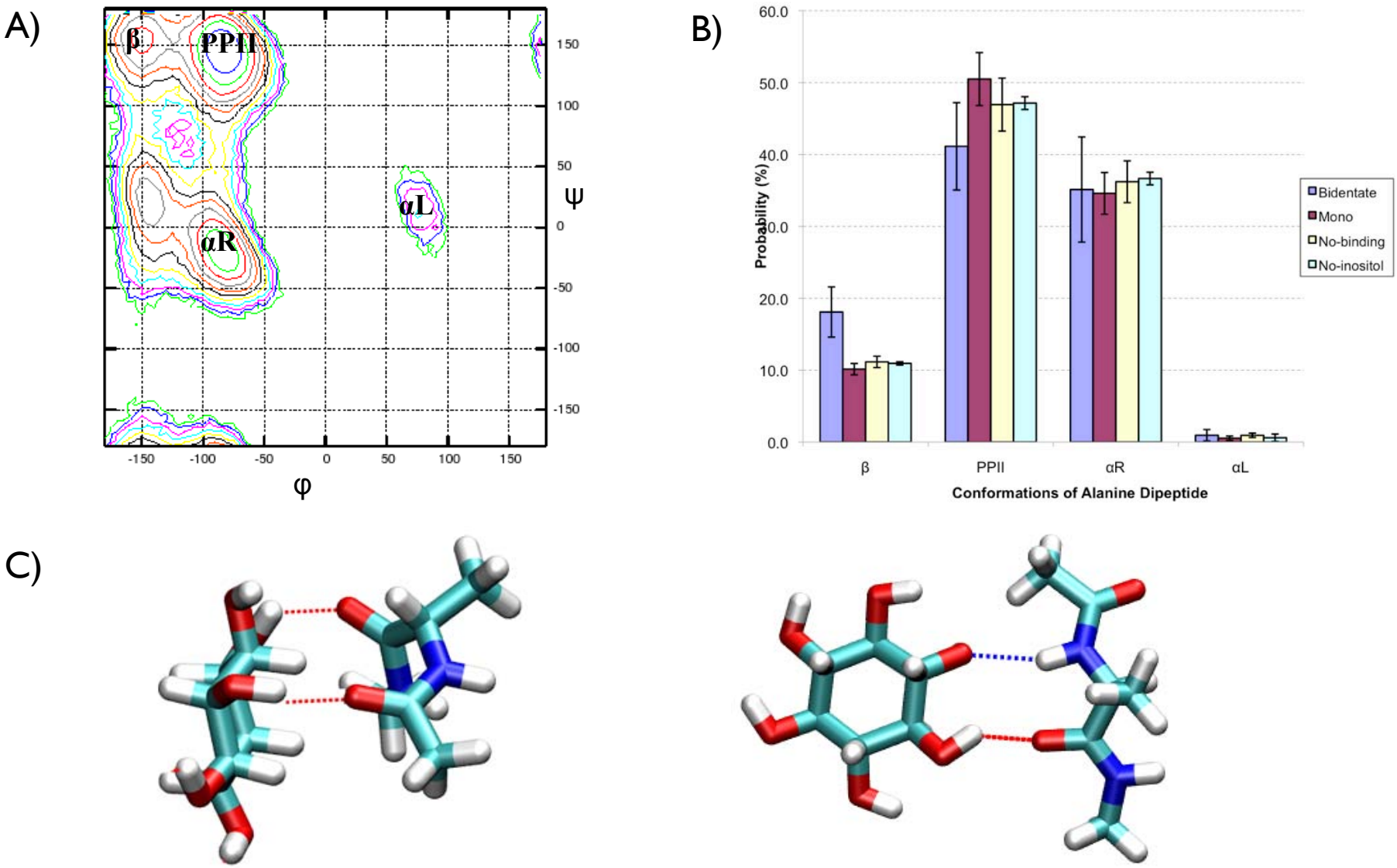

Figure 2: A) The PMF of alanine dipeptide showing the dominant conformations β, PPII, right-handed (αR), and left-handed α-helices (αL). B) Comparisons of bound and unbound populations of scyllo-inositol to alanine dipeptide. C) Examples of bidentate binding modes of scyllo-inositol with β-conformers.

A)

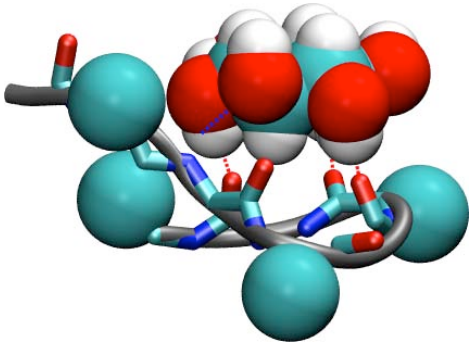

B)

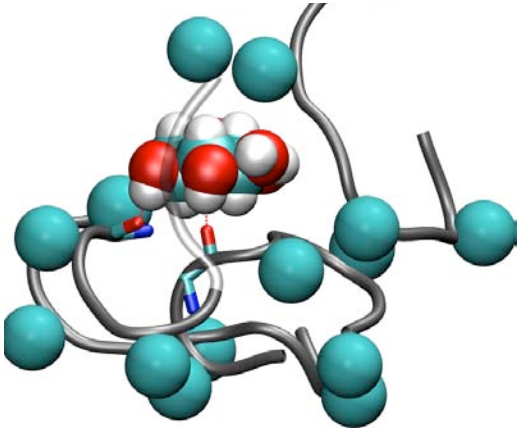

C)

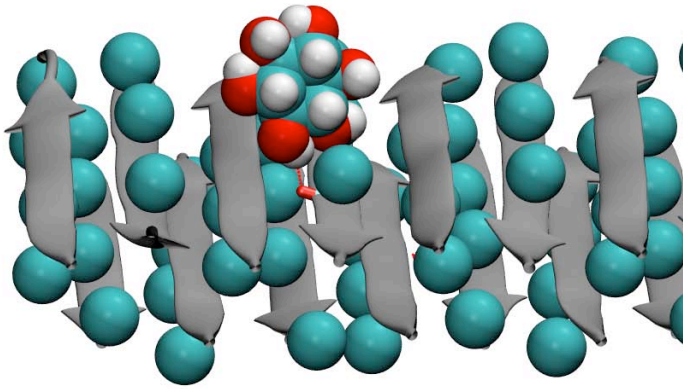

Figure 3: Example snapshots of scyllo-inositol binding to A) monomer B) small oligomer C) β-oligomer of $(GA)_4$:

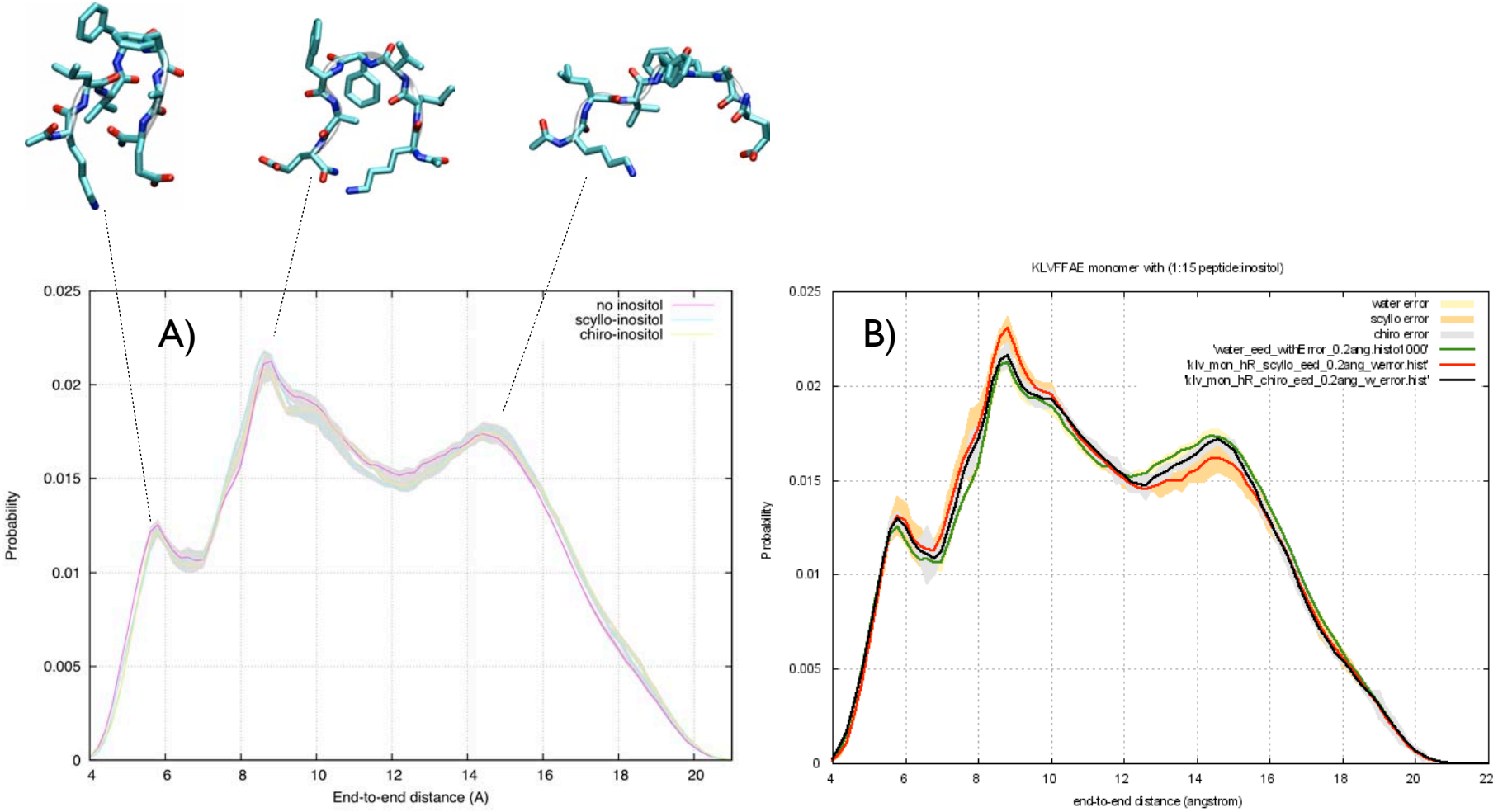

Figure 4: The end to end probability distribution for Aβ(16-22 monomer in absence and in the presence of inositol at molar ratio of A) 2:1 B) 15:1

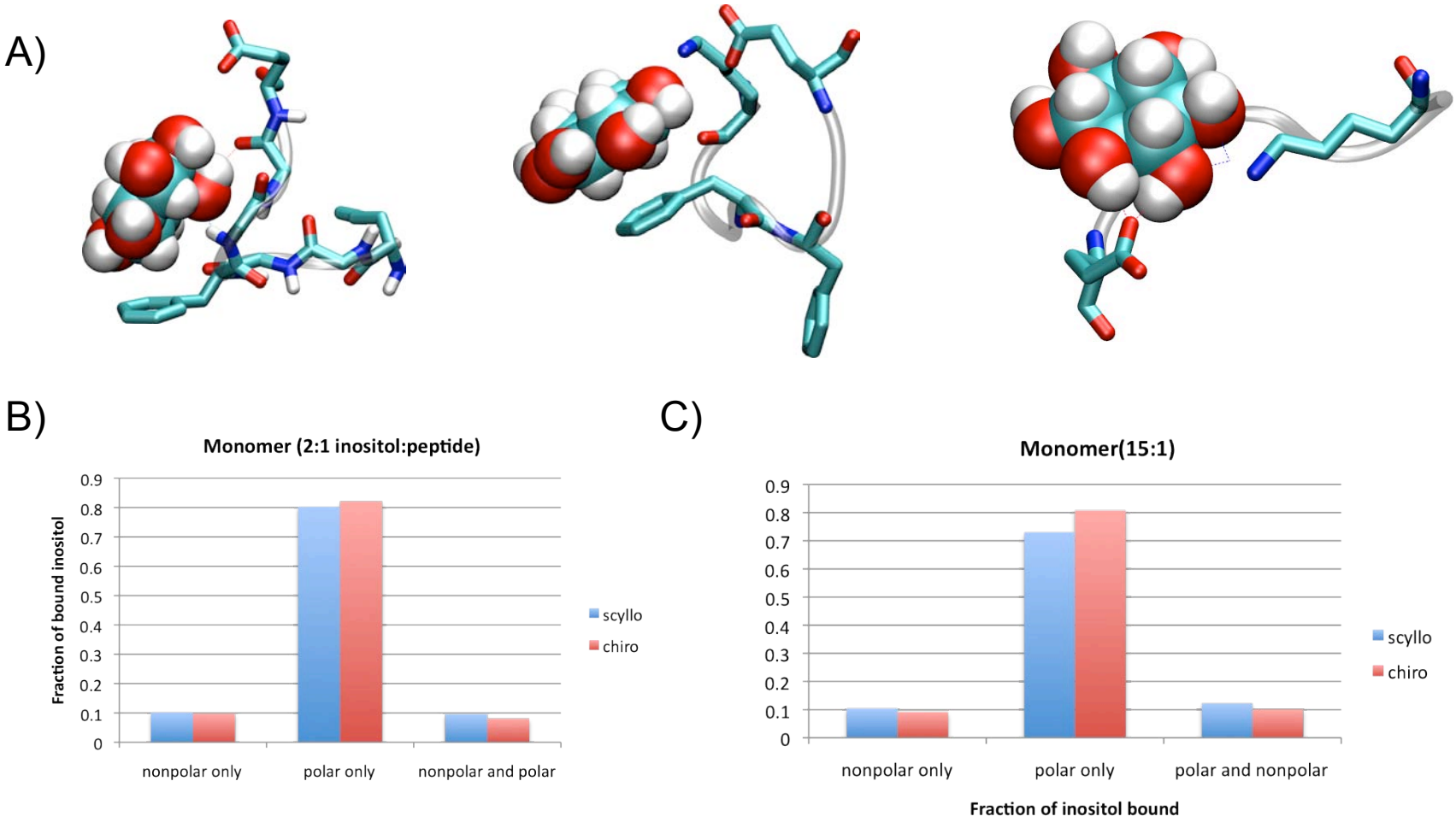

Figure 5: A) Examples of binding modes of inositol to monomer. Fraction of bound inositol at different regions of Aβ(16-22) at B) 2:1 and C) 15:1 inositol:peptide molar ratio.

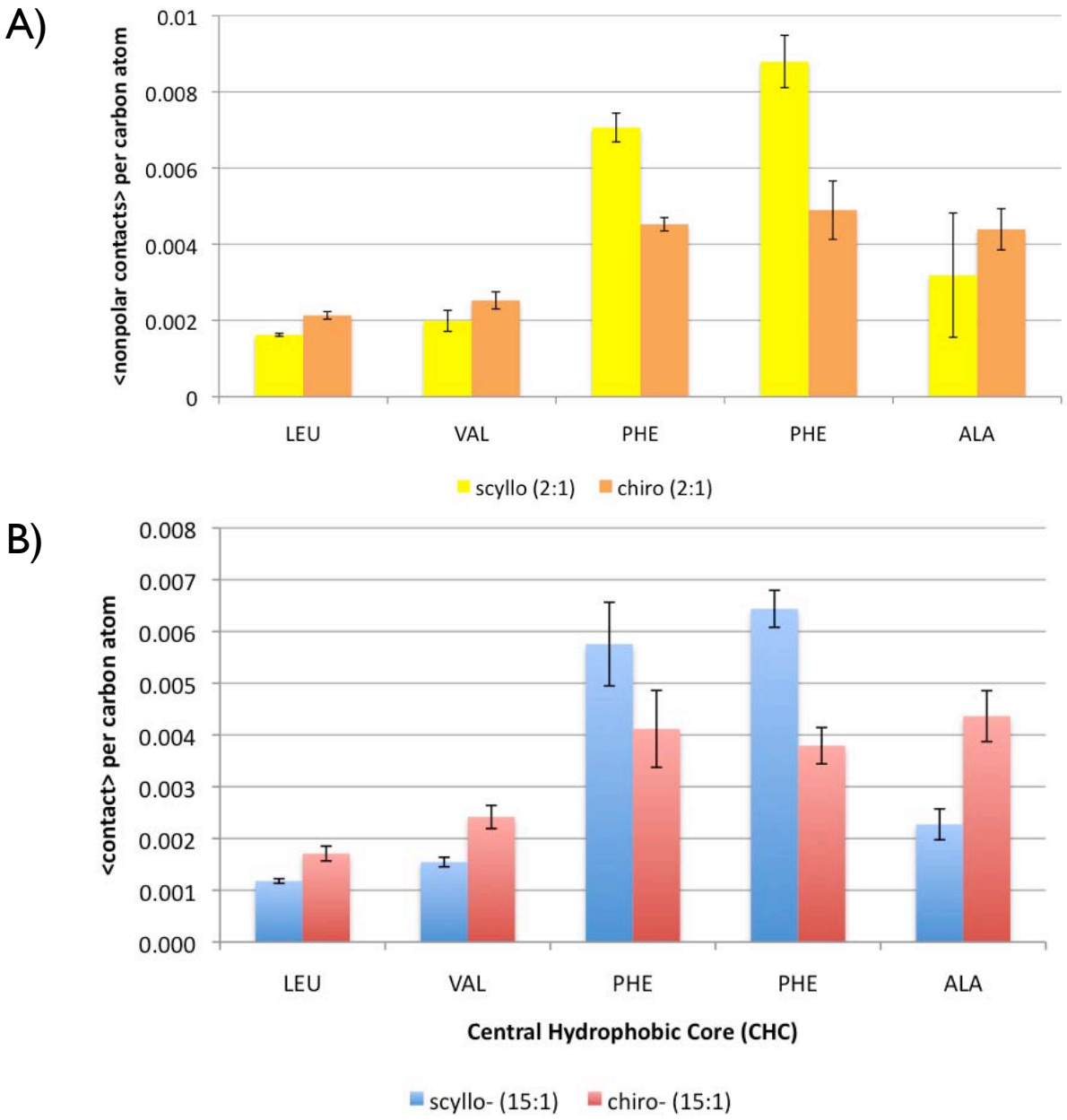

Figure 6: Binding of inositol to the central hydrophobic core (LVFFA) of Aβ(16 to 22) for molar ratios of A) 2:1 and B) 15:1

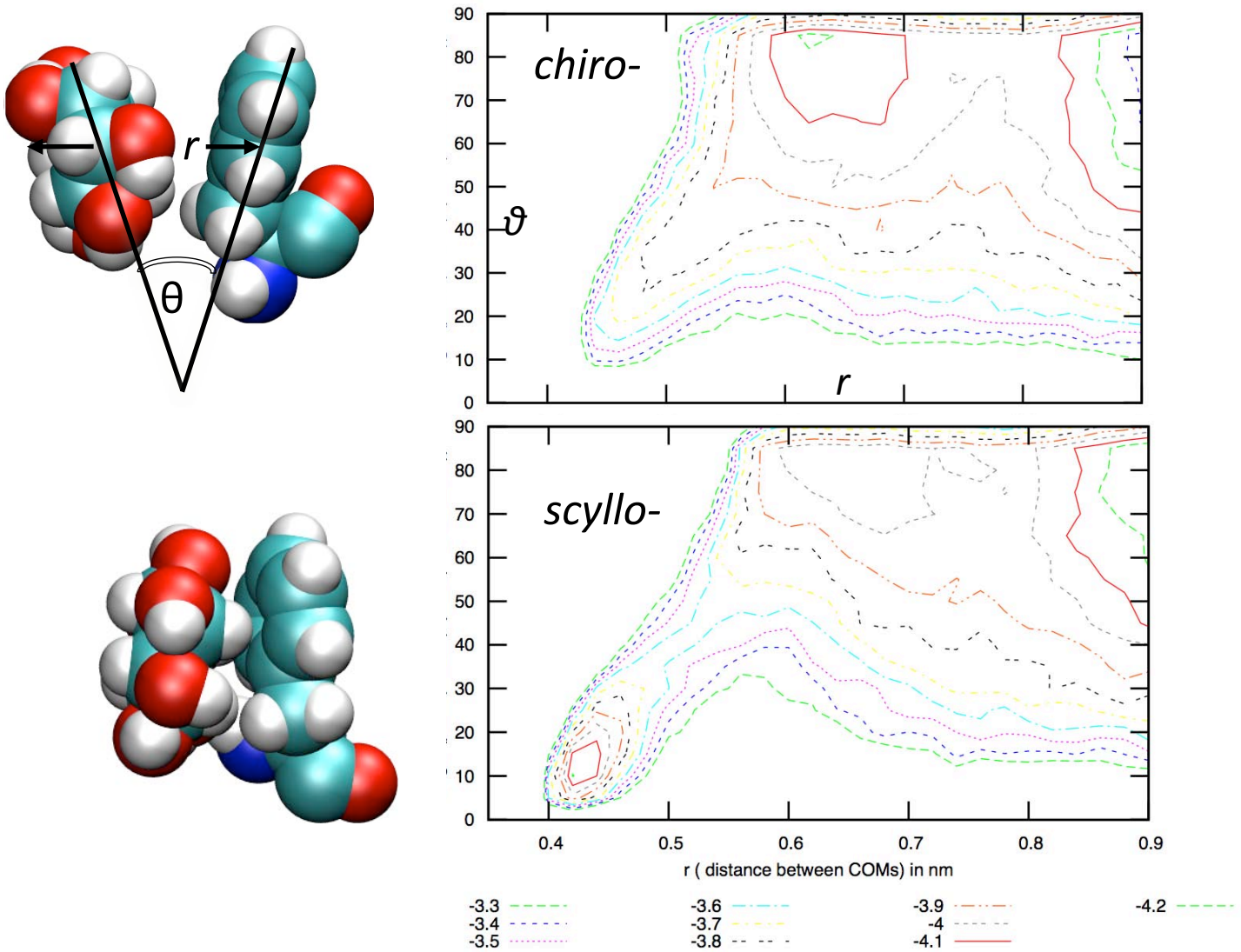

Figure 7: Binding mode of *chiro*- and *scyllo*-inositol with phenyalanines of Aβ(16-22). The potential of mean force of *scyllo*- with the phenyl ring of F shows face to face interaction binding mode at *r*=4.5A and with a planar angle of approx. 12 degrees.

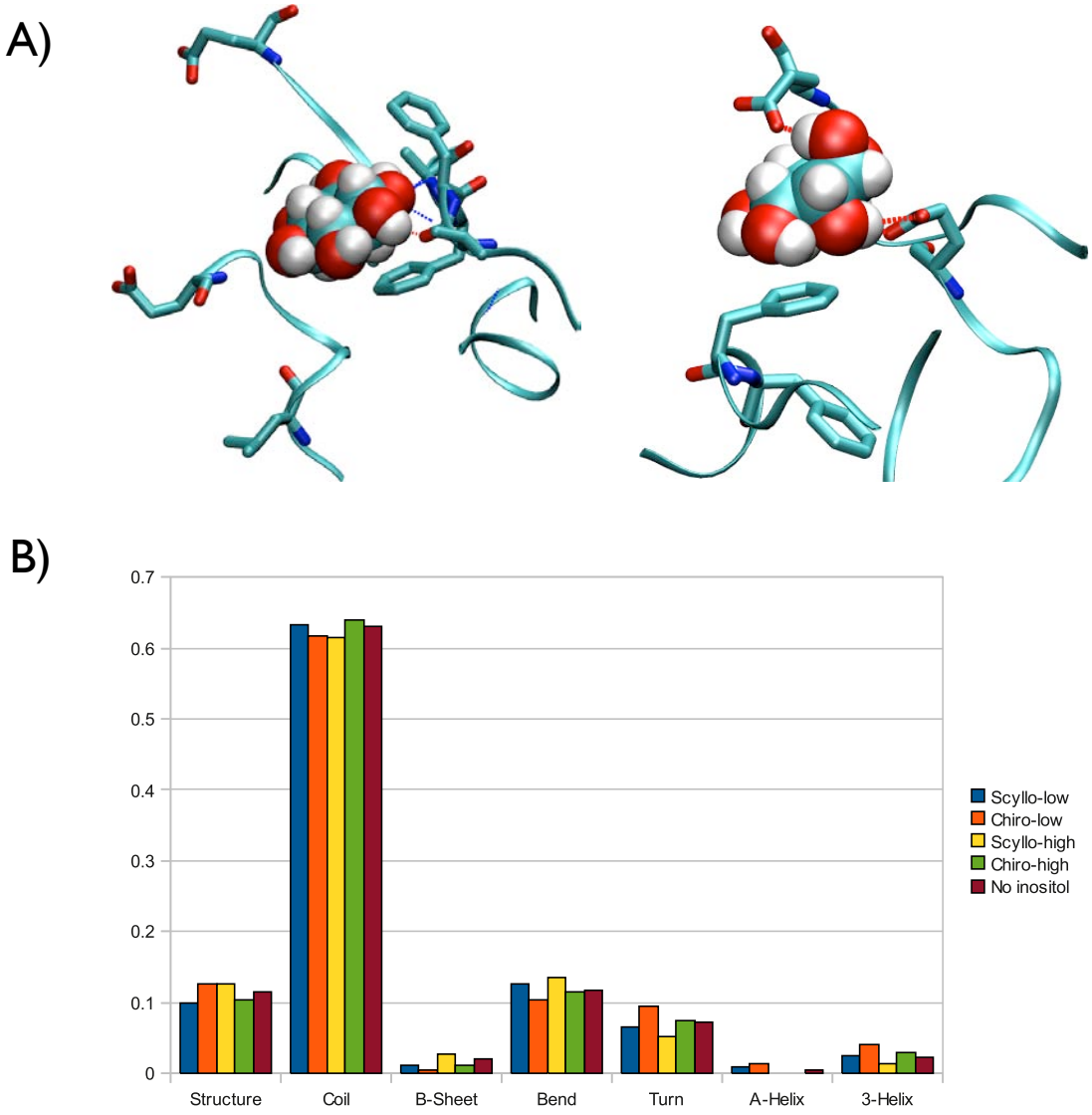

Figure 8: A) Example binding modes of *scyllo*- and *chiro*- to the Aβ(16-22) small oligomer involving both nonpolar and hydrogen bonding. B) The fraction of residues in Structure, Coil, B-Sheet, Bend, Turn , A-helix, 3-Helix for the small oligomer, classified according to DSSP. Note that Structure = B-sheet +Turn + A-Helix + 3-Helix + B-Bridges

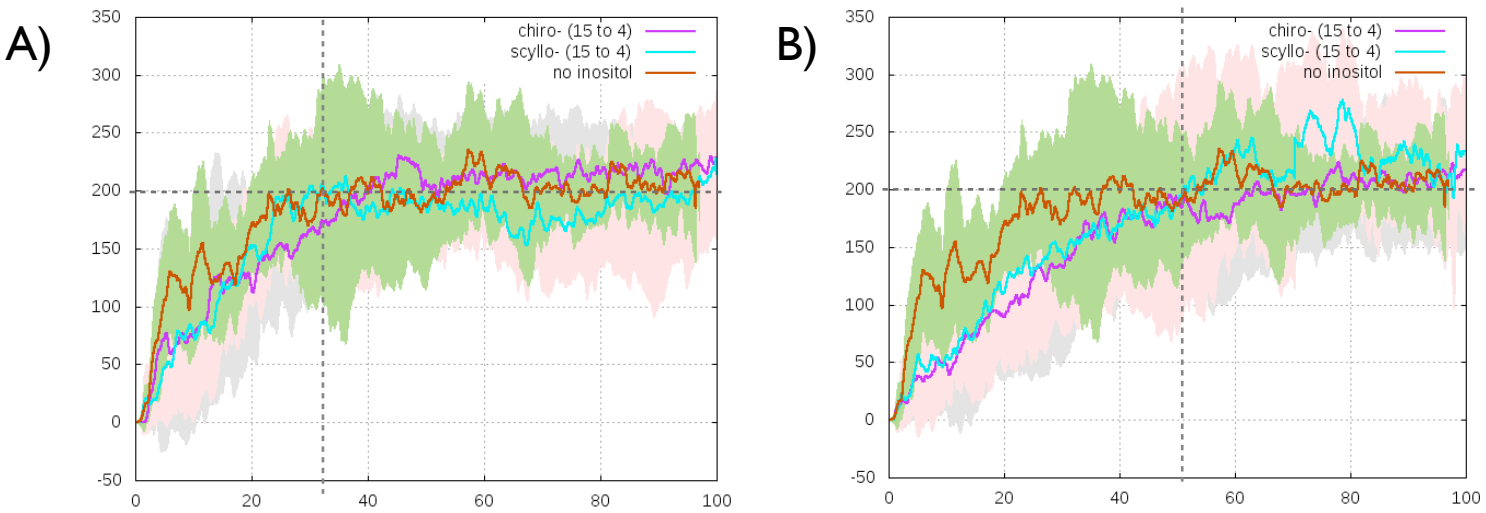

Figure 9: Comparing the hydrophobic association of small oligomer formation in the absence and in the presence of *chiro*- and *scyllo*- at molar ratios of A) 15:4 B) 45:4. Error shaded in Pink = scyllo- Grey = chiro- Green = control (no ino)

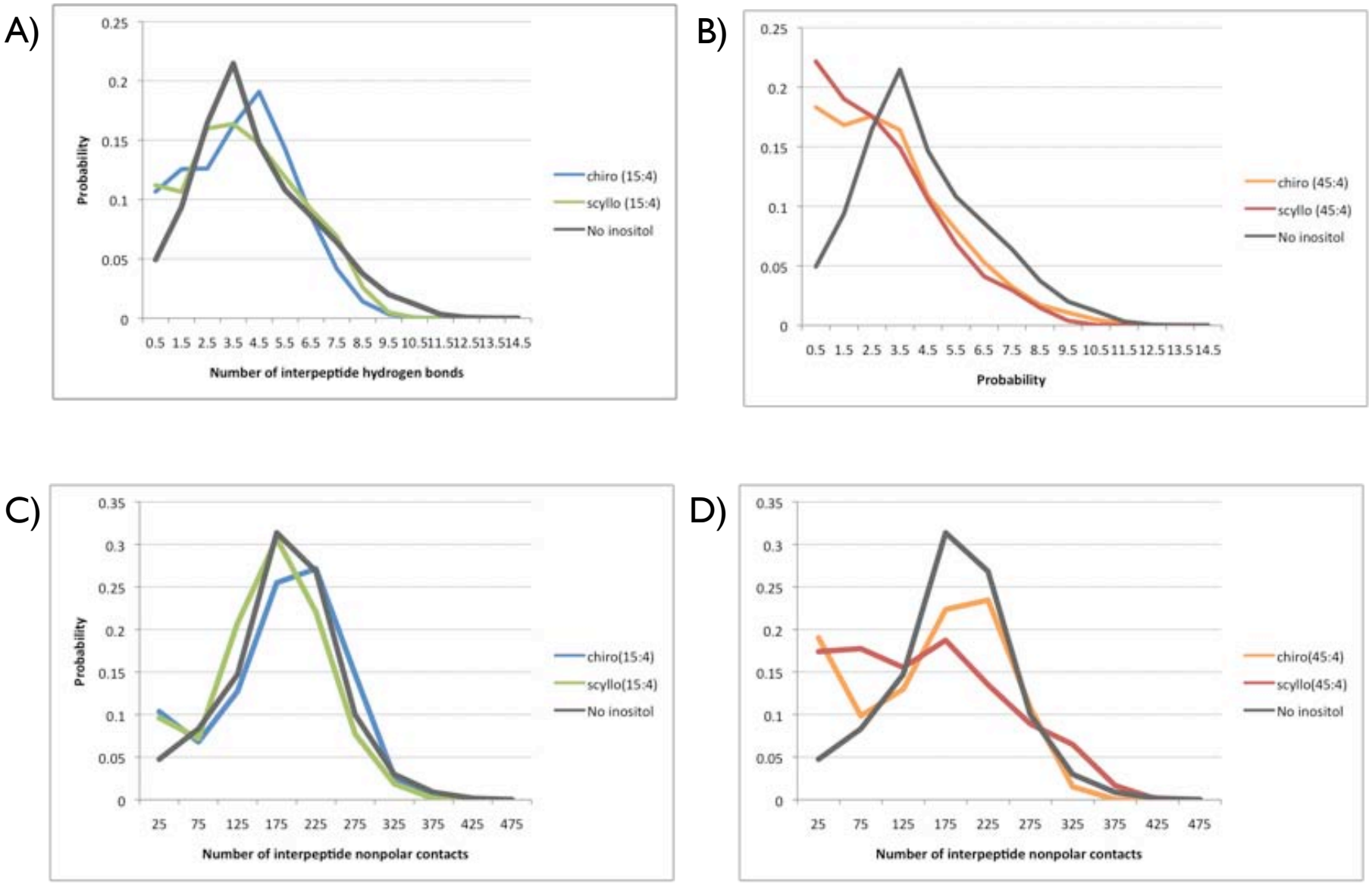

Figure 10: Comparisons of the distribution of interpeptide hydrogen bonding for small oligomers at inositol:peptide molar ratios of A) 15:4 B) 45:4 and the distribution of interpeptide nonpolar contacts at molar ratios of C) 15:4 and D) 45:4.

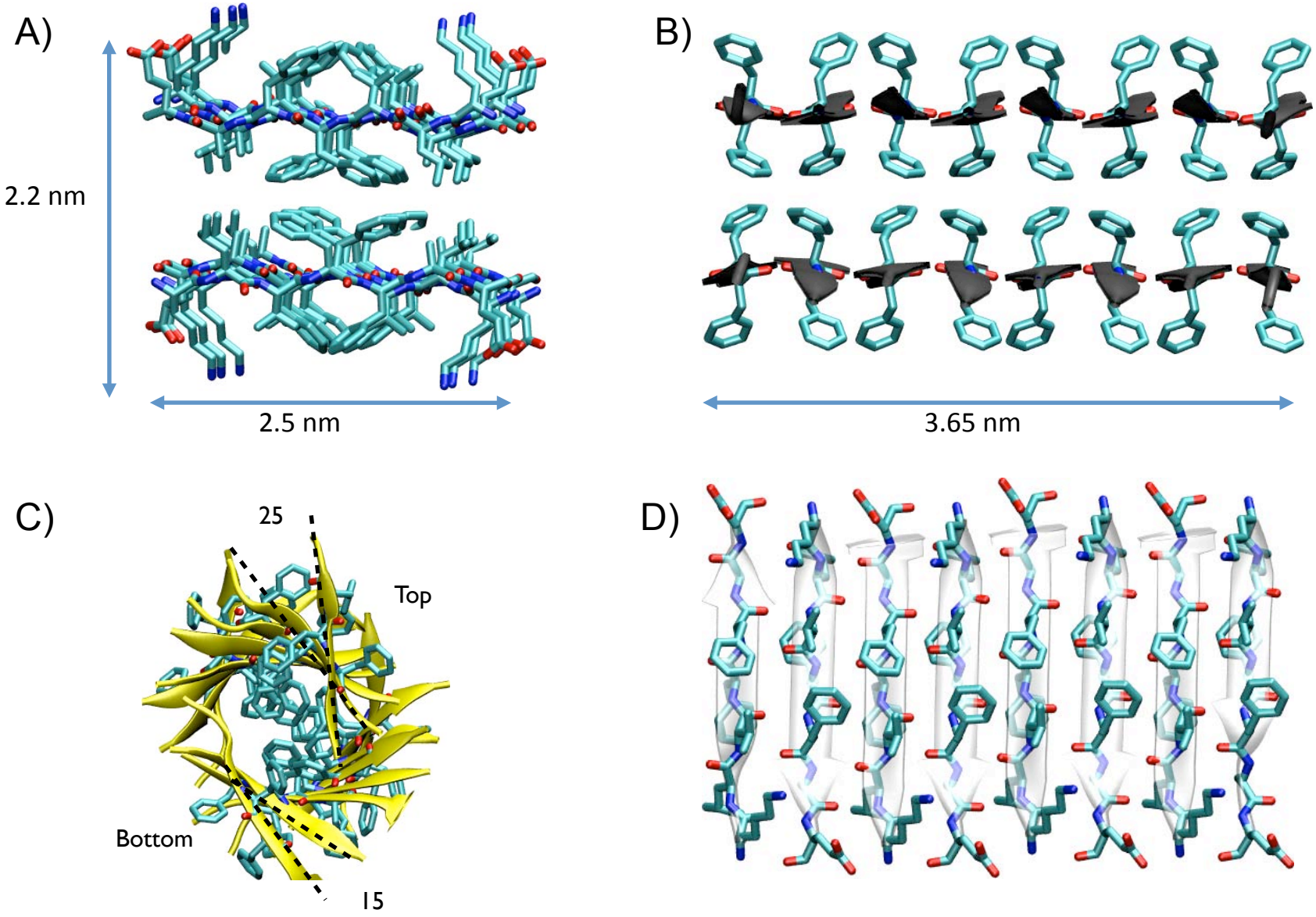

Figure 11: Initial model of the β-oligomer. A) Viewing down along the fibril axis. The height is approx. 22 A and the width is approx. 25 A; B) Viewed from the top at the surface of a sheet. The length is approx. 36.5 A; C) Initial stacking of the sheets. D) Example of the twisted oligomer at simulation time *t*

A)

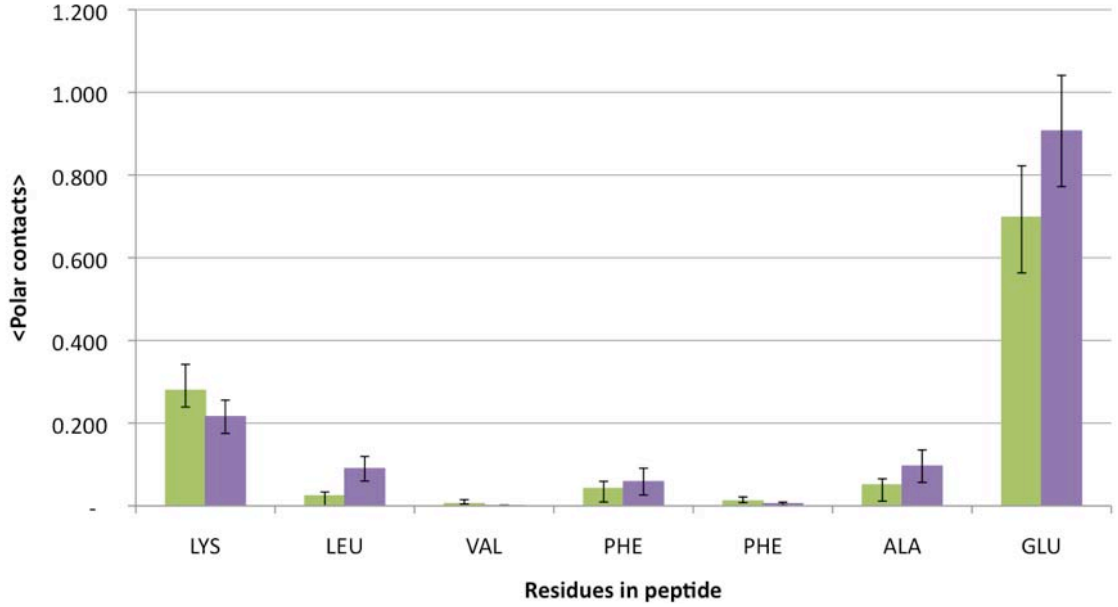

B)

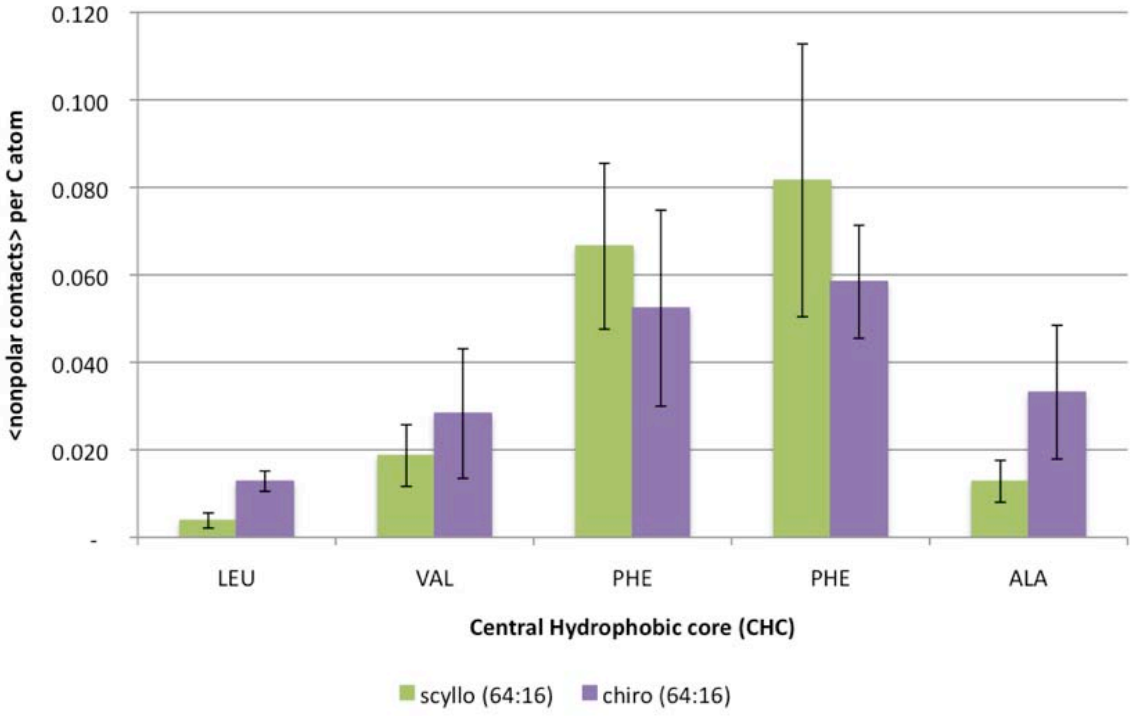

Figure 12: A) Binding of inositol to polar regions (backbone and sidechain) of the beta-oligomer B) Binding of inositol to the central hydrophobic core (LVFFA) of Abeta (16 to 22) beta-oligomer. The inositol:peptide molar ratio is 64:16 and [inositol]=70 mM

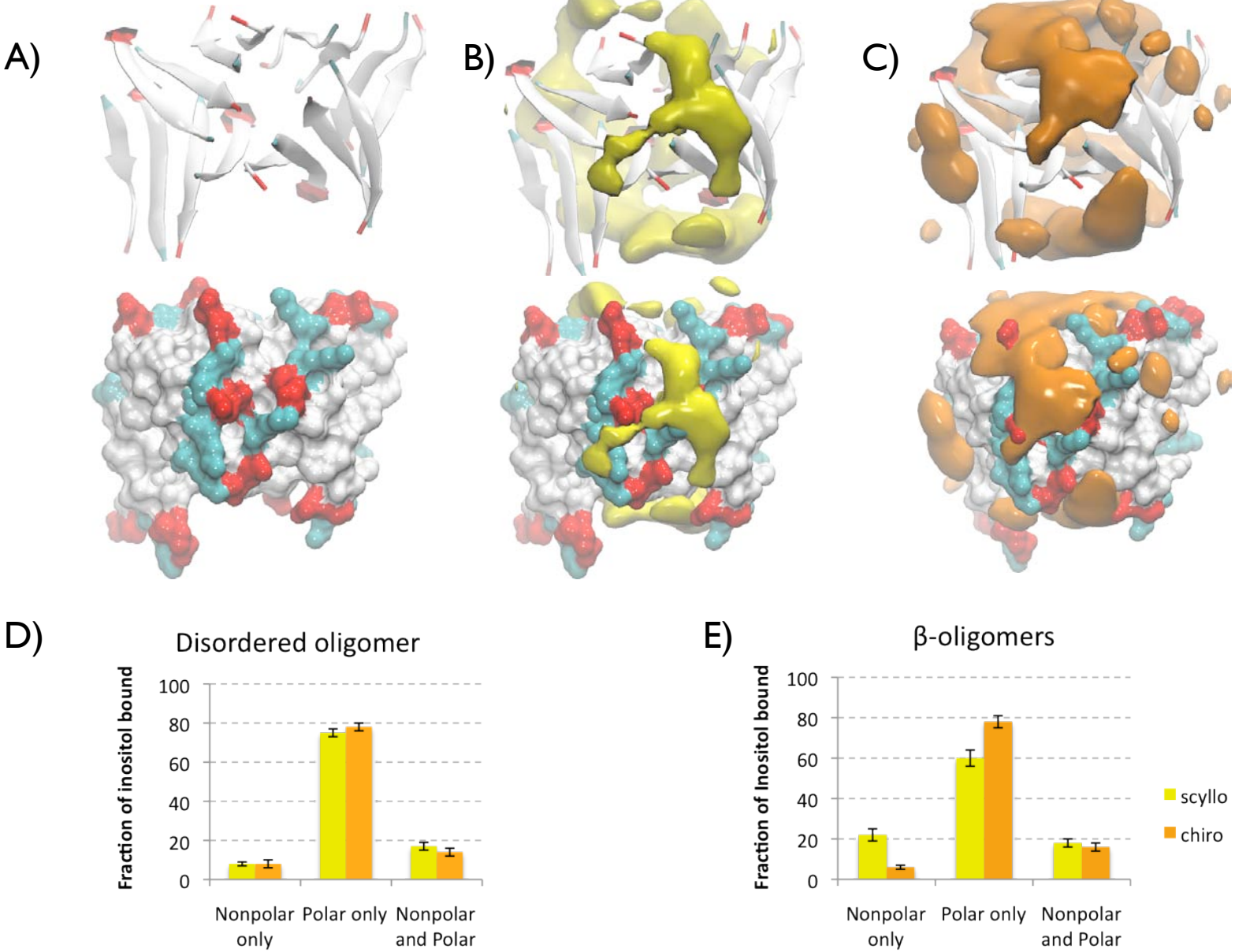

Figure 13: A) The surface representation of the oligomer alone show polar (in green), charged (in red) and hydrophobic (in white) patches. Spatial probability density maps of inositol binding to the β-oligomer of Aβ(16-22) B) *scyllo*-inositol (yellow) C) *chiro*-inositol (orange). Comparisons of fraction of *scyllo*- and *chiro*- bound to different regions of the D) disordered oligomer and E) the β-oligomer.

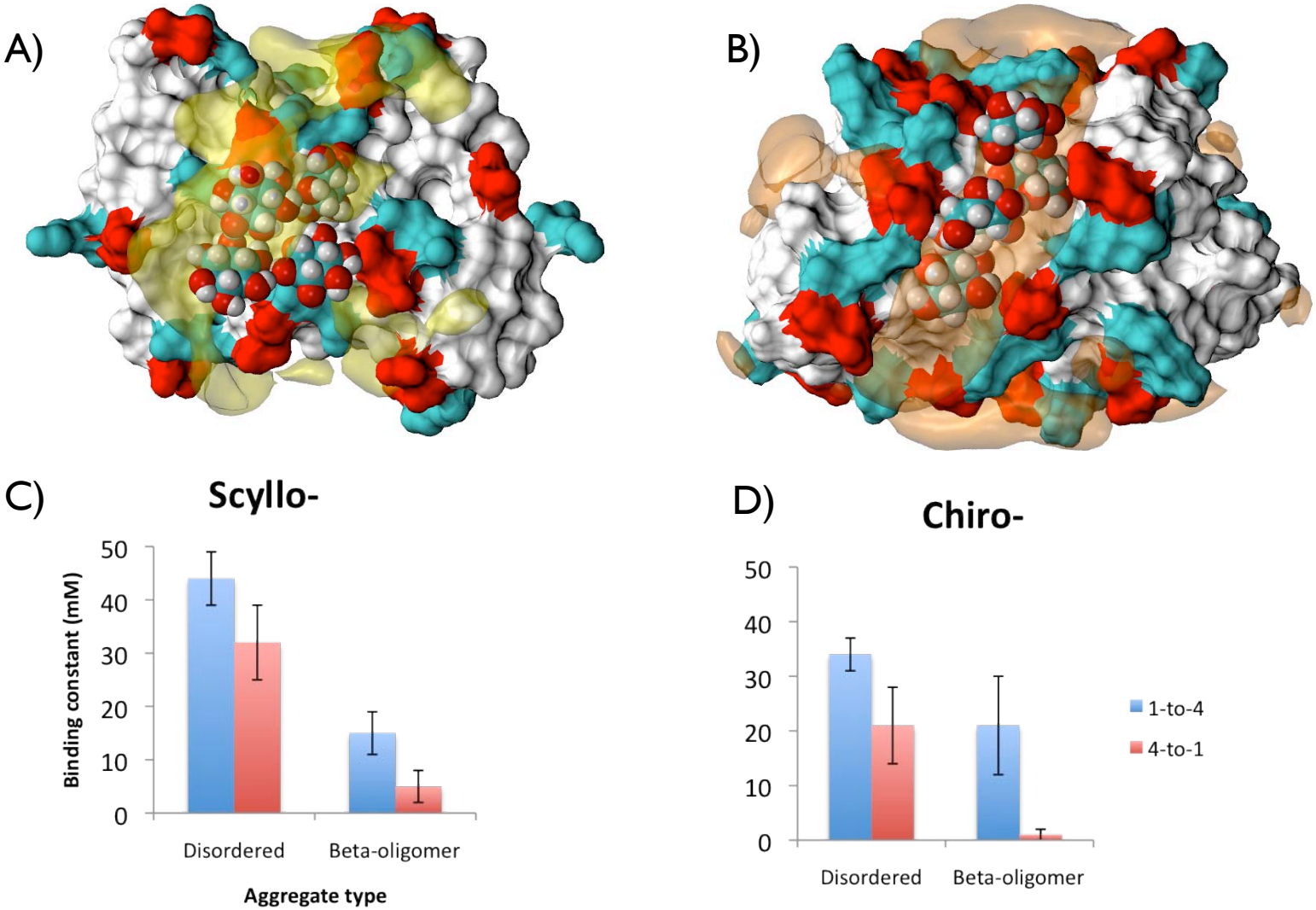

Figure 14: Example of a configuration of a cluster of cooperatively bound *scyllo*-inositol (A) and *chiro*-inositol (B) molecules overlapped with their spatial densities. The comparisons of K_d between lowest and highest molar ratios of C) *scyllo*- and D) *chiro*- for small oligomers and β-oligomers.

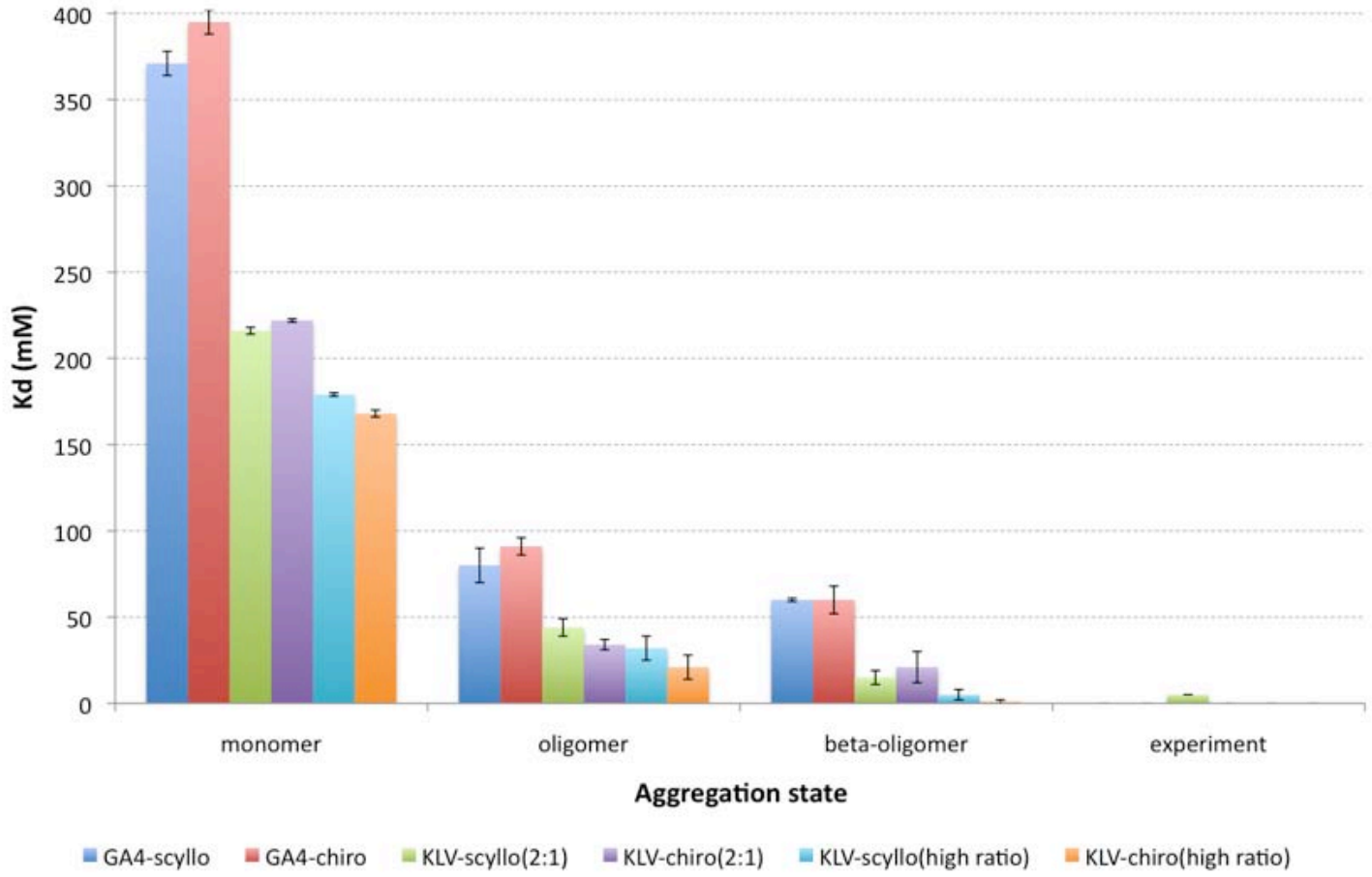

Figure 15: Comparisons of predicted K_d (in mM) of inositol to each of $(GA)_4$ and Aβ(16-22) aggregation states.

System	Kd scyllo in mM (error)	Kd chiro in mM (error)	Num. inositol molecules	Num. peptides	box volume (nm cubed)	box dimensions	[Peptide] (mM)	[INS] (mM)	Inositol:peptide molar ratio	Total simulation time (us)	Number of independent systems
ADP-NONE	N/A	N/A	0	1	27	(3,3,3)	30.8	0	N/A	0.5	5
ADP-INO	1000 mM	1000 mM	4	1	27	(3,3,3)	30.8	123	4:1	0.5	5
GA4M-NONE	N/A	N/A	0	1	27	(3,3,3)	61.5	0	N/A	5	1200
GA4M-INO	371(7)	395(7)	2	1	27	(3,3,3)	61.5	123	2:1	10	2400
GA4DO-NONE	N/A	N/A	0	4	27	(3,3,3)	246	0	N/A	0.5	5
GA4DO-INO	80 (10)	91(5)	2	4	27	(3,3,3)	246	123	2:4 (1:2)	1	10
GA4BO-NONE	N/A	N/A	0	16	61	(4,3.8,4)	440	0	N/A	0.3	3
GA4BO-INO	60(1)	60(8)	4	16	61	(4,3.8,4)	440	110	4:16(1:4)	0.6	6
KLVM-NONE	N/A	N/A	0	1	357.911	(7.1,7.1,7.1)	4.5	0	N/A	5	1200
KLVM-INO-A	216(2)	222(1)	2	1	64	(4,4,4)	61.5	123	2:1	5	1200
KLVM-INO-B	179 (1)	168 (2)	15	1	357.911	(7.1,7.1,7.1)	4.5	70	15:1	5	1200
KLVD-NONE	N/A	N/A	0	4	64	(4,4,4)	104	0	N/A	0.5	5
KLVDO-INO-A	44(5)	34(3)	2	4	64	(4,4,4)	104	52	N/A	1	10
KLVDO-INO-B	32(7)	21(7)	15	4	357.911	(7.1,7.1,7.1)	18	70	15:4 (4:1)	1.6	16
KLVDO-INO-C	N/A	N/A	45	4	357.911	(7.1,7.1,7.1)	18	209	45:4 (12:1)	1.6	16
KLVBO-NONE	N/A	N/A	0	16	180	(6,6,5)	148	0	N/A	0.125	1
KLVBO-INO-A	15(4)	21(9)	4	16	180	(6,6,5)	148	37	4:16(1:4)	1	36
KLVBO-INO-B	5(3)	1(1)	64	16	1728	(12,12,12)	15	62	64:16 (4:1)	1.2	12
KLVBO-INO-C	N/A	N/A	64	16	512	(8,8,8)	52	208	64:16 (4:1)	1.2	12
									Total	41.6	7342

Table 16: Overall summary of computed binding constants for each of the systems simulated in this study